metals

MDPI

Article

Evaluating the Applicability of GTN Damage Model in Forward Tube Spinning of Aluminum Alloy

Xianxian Wang, Mei Zhan *, Jing Guo and Bin Zhao

State Key Laboratory of Solidification Processing, School of Materials Science and Engineering, Northwestern Polytechnical University, Xi'an 710072, China; wangxianx07@163.com (X.W.); guojing_pipi@126.com (J.G.); bzhaonpu@163.com (B.Z.)

* Correspondence: zhanmei@nwpu.edu.cn; Tel.: +86-029-8846-0212-805

Academic Editor: Nong Gao

Received: 20 March 2016; Accepted: 1 June 2016; Published: 6 June 2016

Abstract: Tube spinning is an effective plastic-forming technology for forming light-weight, high-precision and high-reliability components in high-tech fields, such as aviation and aerospace. However, cracks commonly occur in tube spinning due to the complexity of stress state, which severely restricts the improvement of the forming quality and forming limit of components. In this study, a finite element (FE) model coupled with Gurson-Tvergaard-Needleman (GTN) damage model for forward tube spinning of 3A21-O aluminum alloy is established and its applicability is evaluated by experiment. Meanwhile, the GTN damage model is employed to study the damage evolution for forward tube spinning of 3A21-O aluminum alloy. The results show that the FE model is appropriate for predicting the macroscopic crack appearing in uplift area for forward tube spinning, while the damage evolution in deformation area could not be predicted well due to the negative stress triaxiality and the neglect of shear deformation. Accumulation of damage in forward tube spinning occurs mainly in the uplift area. Void volume fraction (VVF) in the outer surface of the tube is higher than that in the inner surface. In addition, it is prone to cracking in the outer surface of tube in the material uplift area.

Keywords: forward tube spinning; 3A21-O aluminum alloy; Gurson-Tvergaard-Needleman (GTN) damage model; finite element (FE) model; crack

1. Introduction

Tube spinning, also known as flow forming, is one of spinning processes widely used to produce cylindrical components with thin-walled section and high precision [1,2]. In this process, the metal is displaced axially along a mandrel, while a continuous and localized plastic deformation is applied by the feeding movement of one or more rollers and rotational motion of the mandrel to reduce the thickness of components [3,4]. According to the relationship between the direction of material flow and roller traversing, the process can be classified as forward and backward tube spinning, as shown in Figure 1 [5]. 3A21 aluminum alloy is one of the most commonly used alloys for aviation, aerospace and automotive industries because of its versatile properties, economical benefit and no need for-heat-treatment advantages [6]. However, due to the highly non-linear feature and complicated stress state during tube spinning, it is prone to cracking in 3A21 aluminum spun parts, which severely restricts the improvement of the forming quality and forming limit of components. Therefore, it is necessary to study the damage evolution of 3A21 aluminum alloy to guide the actual production of spun components.

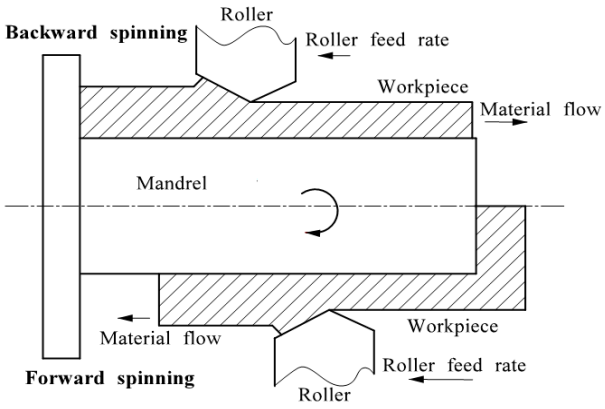

Figure 1. Schematic of forward and backward tube spinning.

Researches on the damage evolution in spinning process coupled with ductile fracture criteria have been reported in recent years. Ma *et al.* [7] investigated the damage evolution in tube spinnability of TA2 titanium tube with nine types of un-coupled ductile fracture criteria in detail. Their result indicated that except for the Freudenthal, Rice and Tracey (R-T) and Ayada models, all the other models can correctly predict the damage distribution on TA2 titanium tube in spinnability test. Cockcroft-Latham (C-L) criterion provided the highest prediction accuracy on the spinnability of TA2 titanium tube, which was only 9% less than the measured experimental value. Zhan *et al.* [8] predicted the failure occurring in shear spin-forming, splitting spin-forming of LF2M aluminum alloy by embedding the Lemaitre and Cockcroft-Latham (C&L) criteria into the finite element (FE) model. The results showed that the Lemaitre criterion was better than the C&L criterion at accurately predicting the position at which damage will occur. A thermal damage model for tube spinning process of Ti-6Al-2Zr-1Mo-1V combining the Oyane ductile fracture criterion with the relationship among damage threshold, temperature and strain rate was also established by Zhan *et al.* [9]. Their results indicated that the inner surface of the spinning region was the zone most prone to damage due to positive stress triaxiality and large strain rate.

Recently, studies on expansion and accumulation of cavities in ductile material have been carried out. It is often believed that, the ductile failure process of metal material consists of three stages in mesoscopic scale: micro-voids nucleation, growth and coalescence, respectively [10,11]. The typical model to describe these three stages is the Gurson-Tvergaard-Needleman (GTN) damage model, which is proposed by Gurson [10] and further modified by Tvergaard and Needleman [11]. Compared with other ductile fracture criteria, GTN damage model is a coupled ductile fracture criterion, incorporating the void evolution into the constitutive equations. Generally, GTN damage model and modified GTN damage model are applied to predict void initiation, propagation, and final rupture [12,13] combined with FE simulation in some process. Chen and Dong [12] predicted the damage in deep drawing test of AA6111 aluminum alloy well with a modified GTN yield criterion based on a quadratic anisotropic yield criterion and an isotropic hardening rule. Butcher *et al.* [13] predicted the burst pressure, formability and failure location in tube hydroforming of dual phase (DP600) steel using GTN constitutive model and interpreted the influence of void shape and shear on coalescence. Sun *et al.* [14] analyzed the ductile damage and failure behavior of steel sheet with edge defects under multi-pass cold rolling based on the shear GTN damage model proposed by Nahshon and Hutchinson [15]. Li *et al.* [16] indicated that the GTN damage model can predict the damage in tube bending process. However, it cannot predict the damage evolution due to the negative stress triaxiality in split spinning. It can be found that most of these studies about GTN damage model concentrate on the simple stress state. Researches on GTN damage model applied in other complicated deformation, such as tube spinning process, are limited. In tube spinning process, many researches on damage evolution have been studied based on other ductile fracture criteria. However, there are few researches on damage

evolution based on GTN damage model in this process. Thus, the applicability and limitation of GTN damage model in tube spinning should be evaluated in detailed.

To investigate the applicability of GTN damage model to predict fracture in tube spinning process, an FE model coupled with GTN damage model for forward tube spinning of 3A21-O aluminum alloy is established based on ABAQUS/Explicit platform. Then the applicability of GTN damage model in spinning process is evaluated by experiment. Distributions of the stress triaxiality, the maximum principal stress, and the void volume fraction (VVF) are analyzed to reveal damage evolution in forward tube spinning finally.

2. Material and Methods

The material used in this study is 3A21-O aluminum alloy. The chemical composition of the alloy is listed in Table 1. Parameters of the material are shown in Table 2.

Table 1. Chemical composition of 3A21-O aluminum alloy.

Position	Si	Fe	Cu	Mn	Mg	Zn	Ti	Al
Mass fraction (%)	0.6	0.7	0.2	1.3	0.05	0.10	0.15	Bal.

Table 2. Material parameters of 3A21-O aluminum alloy.

Parameters	Values
Elastic modulus (GPa)	69.98
Poisson's ratio	0.33
Yield strength (MPa)	52
Strength coefficient (MPa)	188.76
Hardening exponent	0.194

Based on the ABAQUS/Explicit platform, uniaxial tensile simulations under the same condition as experiments are conducted to determine main parameters in GTN damage model. Tensile tests are carried out on a CMT5205 electronic universal testing machine (MTS Systems Corporation, Eden Prairie, MN, USA) at a maximum load of 200 KN. Dimensions of uniaxial tensile test specimen are shown in Figure 2. Experiments of forward tube spinning are carried out on a CZ900/CNC spin forming machine (Sichuan Space Industry Company, China). Taking the large size of the blank in experiment into consideration, theory of similarity [17] is adopted to improve the efficiency of calculation in simulation. The ratio of similitude is 4 in this study. The main process parameters in experiment and simulation for forward tube spinning are listed in Table 3. In order to analyze the damage evolution in forward tube spinning, the tube is divided into four areas, namely un-deformed area, uplift area [9], deformation area, and deformed area, respectively (Figure 3).

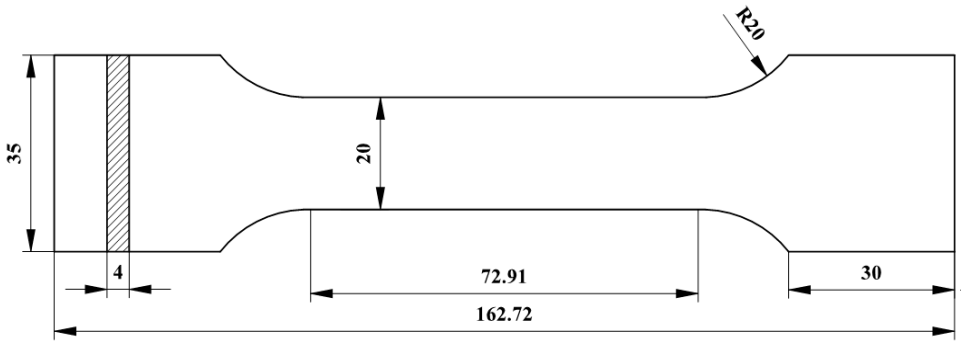

Figure 2. Dimensions of uniaxial tensile specimen (Unit: mm).

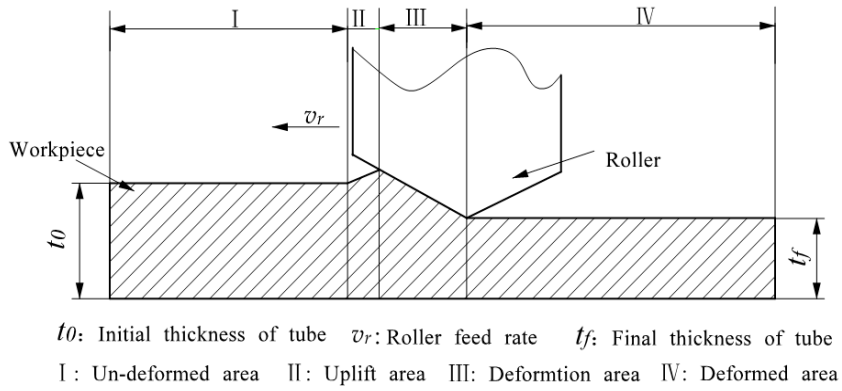

Figure 3. Schematic of area division of the tube in forward spinning.

Table 3. Process parameters in simulation and experiment.

Parameters	Experiment	Simulation
Inner diameter of the tube d (mm)	320.6	80.15
Thickness of the tube t_0 (mm)	12	3
Initial height of the tube h (mm)	150	37.5
Roller nose radius r (mm)	5	1.25
Roller feed rate v_r (mm/r)	1.25	0.3125
Roller attack angle α (°)	30	30
Mandrel rotational speed ω (r/min)	100	100
Reduction ratio of wall thickness Ψ (%)	50	50

3. Gurson-Tvergaard-Needleman (GTN) Damage Model and Finite Element (FE) Model in Tube Spinning

3.1. GTN Damage Model

The Gurson model revised by Tvergaard and Needleman, namely the GTN damage model, can be expressed as Equation (1) [10,11]:

$$\phi(\sigma, f) = \left(\frac{\sigma_{eq}}{\sigma_y}\right) + 2q_1 f^* \cosh\left(-\frac{3q_2\sigma_m}{2\sigma_y}\right) - \left(1 + q_3 f^{*2}\right) = 0 \quad (1)$$

where, ϕ is the yield function; σ_{eq} is the von Mises equivalent stress; σ_y the mean uniaxial equivalent stress of the matrix material; σ_m is macroscopic hydrostatic pressure; f is the VVF; q_1, q_2 and q_3 are the constants for material. When $q_1 = q_2 = q_3 = 1$, Equation (1) can be degraded into the Gurson model. f^* is the modified void volume fraction that takes into account the final decrease in load when void coalescence occurs. The relationship between f^* and f is given as follows:

$$f^* = \begin{cases} f \ (f \leqslant f_c) \\ f_c + \frac{1/q_1 - f_c}{f_F - f_c}(f - f_c) \ (f_c < f < f_F) \end{cases} \quad (2)$$

where, f_c is the critical VVF when the void coalescence takes place and f_F is the VVF at the final failure of material.

The evolution of voids is characterized by the gradually growth of existing voids volume fraction (f_g) and nucleation of new voids volume fraction (f_n) in material, as shown in Equation (3):

$$df = df_g + df_n \quad (3)$$

The void growth rate is determined by the plastic incompressibility of matrix surrounding the voids with respect to the rule of mass balance in representative volume elements. It can be expressed as Equation (4):

$$\mathrm{d}f_g = (1-f)\mathrm{d}\varepsilon^p : 1 \tag{4}$$

where, $\mathrm{d}\varepsilon^p$ is the increment of hydrostatic plastic strain and I is a second order unit tensor.

The growth of strain controlled nucleation of new voids [18] can be expressed as Equation (5):

$$\mathrm{d}f_n = A\mathrm{d}\varepsilon_y{}^{pl} \tag{5}$$

with $A = \frac{f_n}{S_n\sqrt{2\pi}}\exp\left[-\frac{1}{2}\left(\frac{\varepsilon_y{}^{pl}-\varepsilon_n}{S_n}\right)^2\right]$, where, f_n is the total void volume fraction that can be nucleated; ε_n is the mean equivalent plastic strain for void nucleation; S_n is the corresponding standard deviation and $\mathrm{d}\varepsilon_y{}^{pl}$ is the increment of equivalent plastic strain.

3.2. Determination of Parameters in GTN Damage Model

In the GTN model, q_1, q_2, q_3, ε_n and S_n can be determined by empirical values, and f_0, f_n, f_c and f_F are generally determined by scanning electron microscope (SEM) microstructures. In this study, to reflect the interaction in two void groups in GTN model, values of q_1, q_2 and q_3 are quantified as 1.5, 1 and 2.25, respectively [19]. The value of S_n is determined as 0.1 and ε_n is assigned as 0.3 [10,12,20]. Considering that there are many researches on the GTN damage model of aluminum alloy, the microstructure of 3A21 aluminum alloy can be hardly observed due to its excellent corrosion resistance, the initial void volume fracture f_0 is determined as 0.001 according to the values adopted in other aluminum alloy [12,21], and f_n, f_c and f_F are determined by anti-inference method [21] through the combination of experiment with FE simulation of uniaxial tensile test.

The true stress strain curves in experiment and in simulation with different parameters in the GTN model (Table 4) are shown in Figure 4. It can be seen that, under the same dimensions of specimen and loading condition, different parameters in the GTN damage model have significant effects on the deformation behavior of material. In experiment, ultimate tensile strength reaches to 143.13 MPa at the strain of 0.27. When the strain is larger than 0.27, there are obvious differences in stress strain curves between simulation and experiment. Considering that the specimen bears the maximum load and void coalescence begins, and the hardening properties decrease suddenly due to the coalescence of void speed which depends on the factor f_F [22], stress strain curves between simulation and experiment can be compared by critical strain (strain corresponding to tensile strength) and fracture strain. When the strain is less than 0.27, stress strain curves in simulation are similar to each other. The differences of stress strain curves between simulation and experiment in this region can be symbolized as standard deviation (*SD*), which can be expressed as:

$$SD = \sqrt{\frac{\sum_{i=1}^{n}(x_i - x_{irel})^2}{n}} \tag{6}$$

where, x_i is the stress in simulation at a certain strain (0.02, 0.04, 0.06,...,0.26); x_{irel} is the stress in experiment at the corresponding strain; n is 13 in this study.

Standard deviation, critical strain and fracture strain under different parameters in the GTN model are shown in Table 4. It can be seen that there are minimum standard deviation under the parameters in group 5. Meanwhile, in simulation critical strain and fracture strain under these parameters are also closer to those in experiment. Thus, in this study, f_n, f_c and f_F are determined as 0.012, 0.02 and 0.04, respectively.

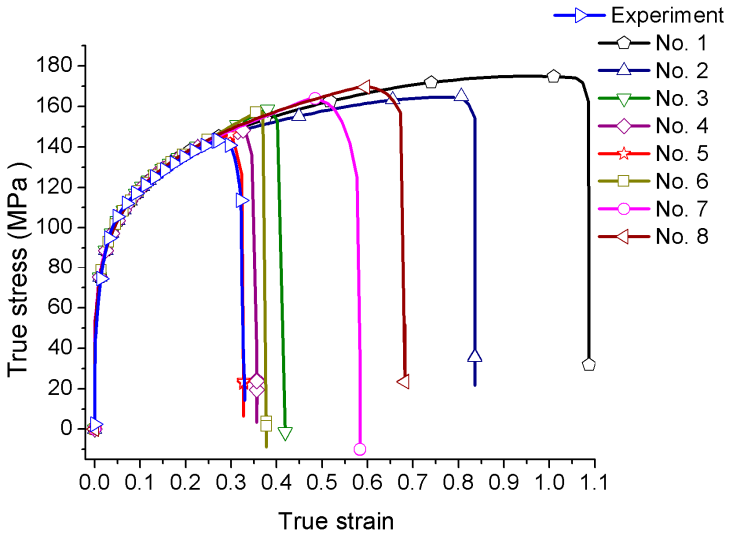

Figure 4. True stress strain curves of different parameters coupled with Gurson-Tvergaard-Needleman (GTN) damage model.

Table 4. Standard deviation, critical strain and fracture strain under different parameters in Gurson-Tvergaard-Needleman (GTN) damage model.

Values \ Group	1	2	3	4	5	6	7	8	Experiment
f_n	0.01	0.02	0.02	0.015	0.012	0.01	0.04	0.002	-
f_c	0.05	0.05	0.02	0.02	0.02	0.01	0.05	0.005	-
f_F	0.1	0.1	0.05	0.04	0.04	0.02	0.15	0.05	-
Standard deviation	1.47	1.30	1.70	1.26	1.25	1.75	1.36	1.72	-
Critical strain	1.01	0.81	0.38	0.32	0.30	0.35	0.48	0.59	0.27
Fracture strain	1.09	0.84	0.42	0.36	0.33	0.38	0.58	0.68	0.33

3.3. Establishment of the FE Model for Forward Tube Spinning Coupled with GTN Damage Model

Based on the ABAQUS/ Explicit platform, an FE model coupled with the GTN damage model for forward tube spinning process of 3A21-O aluminum alloy is established, as shown in Figure 5. In the model, rollers and mandrel are assumed to be analytical rigid bodies. The tube is considered as a deformable body, which is meshed by an 8-node linear brick, reduced integration and hourglass control element (C3D8R). Five layer elements are divided in the thickness direction of the tube because five layer elements are enough to get the variation information of wall thickness during spinning [17]. Three simulations with mesh sizes of 1, 1.5 and 2 mm in the axial-hoop plane are compared, as shown in Table 5. The mass scaling is 2000 to ensure the efficiency and accuracy in simulation. As seen in Table 5, there are small increases of maximum Mises stress and maximum equivalent strain with mesh size decreasing. However, central processing unit (CPU) time is increased obviously with mesh size decreasing. Considering the efficiency and accuracy of simulation, mesh size of 1.5 mm in the axial-hoop plane are adopted in this study. Coupling constraint is adopted to limit the movement of bottom surface of tube in simulation. Arbitrary Lagrangian-Eulerian (ALE) adaptive grid technique is used to avoid the distortion of the mesh and birth-and-death element is adopted to delete the element whose VVF exceeds f_F. The GTN damage model is implanted into forward tube spinning through the porous metal plasticity module in ABAQUS platform.

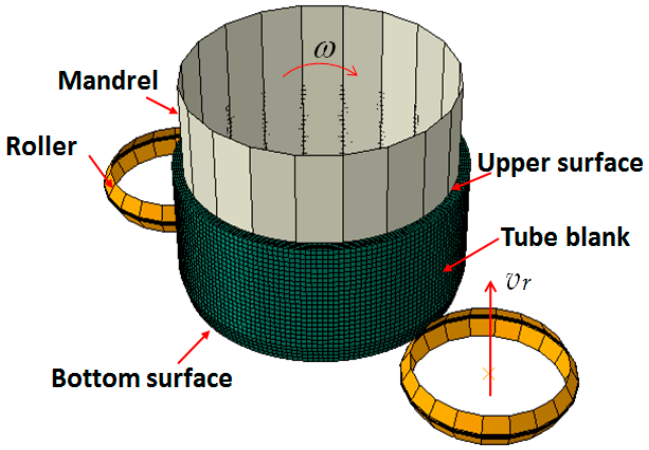

Figure 5. The finite element model for forward tube spinning.

Table 5. Simulation results under different mesh sizes.

Simulation results	Mesh Size		
	2 mm	1.5 mm	1 mm
Maximum Mises stress (MPa)	238.4	239.1	239.1
Maximum equivalent strain	2.826	3.276	3.41
Central processing unit time (h)	68	128	244

4. Evaluating the Applicability of the FE Model Coupled with GTN Damage

To verify the reliability of the FE model coupled with GTN damage model for forward tube spinning of 3A21-O aluminum alloy, the energy variation of the FE model are evaluated and corresponding experiments are carried out. Figure 6 shows the variations of kinetic energy and the ratio of kinetic energy to internal energy in forward tube spinning. It is found that, the variation of kinetic energy is stable except for the initial stage of forward tube spinning, and the ratio of kinetic energy to internal energy is less than 5% during most stage of the forward tube spinning, which indicate that the FE model is theoretically reliable [23].

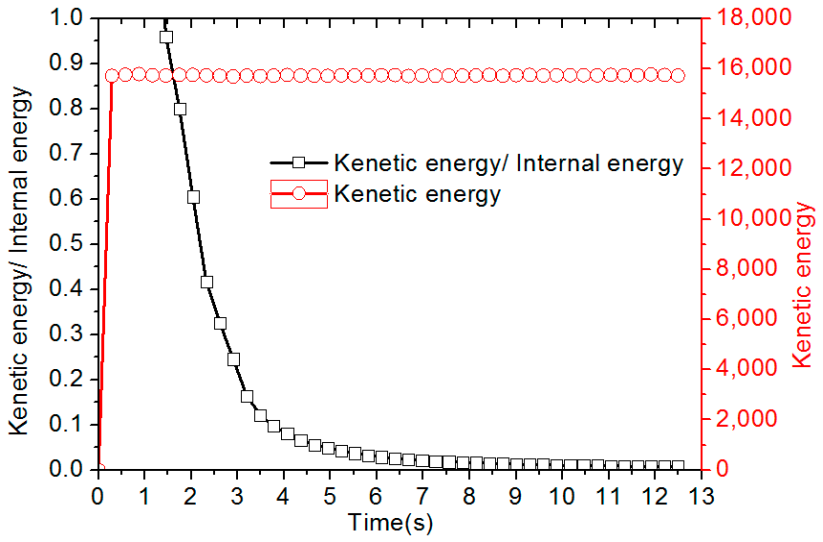

Figure 6. Energy evaluated of finite element model for forward tube spinning of 3A21-O aluminum alloy.

To evaluate the applicability of the GTN damage model in forward tube spinning in this study, experiments are conducted under the parameters as shown in Table 3. Figures 7 and 8 show the crack defects of the tube in simulation and in experiment at wall thickness reduction ratio of 50%. It can be seen that, in the outer surface of tube, some elements are deleted in the material uplift area and bottom area (Figure 7a) due to the birth-and-death element adopted when the VVF exceeds the f_F. Cracks are not observed in the inner surface of tube in simulation (Figure 7b). This indicates that in simulation, macroscopic cracks mainly occur in the material uplift area. Cracks appearing in the bottom region of tube in simulation are not emphasized in this study, because they are generated mainly due to the complicated and large force when the coupling constraint is adopted to limit the movement of the bottom surface in simulation. In experiment process, penetrating cracks (Area 1) are found in deformed area (Figure 8a,b). Except for the penetrating cracks, there is no crack in the inner surface of tube. Localized magnification image (Figure 8c) of Area 2 in Figure 8a indicates there are also many tiny cracks occurring in the material uplift area. Meanwhile, both in simulation and experiment, cracks are more serious at the peak of the material uplift area.

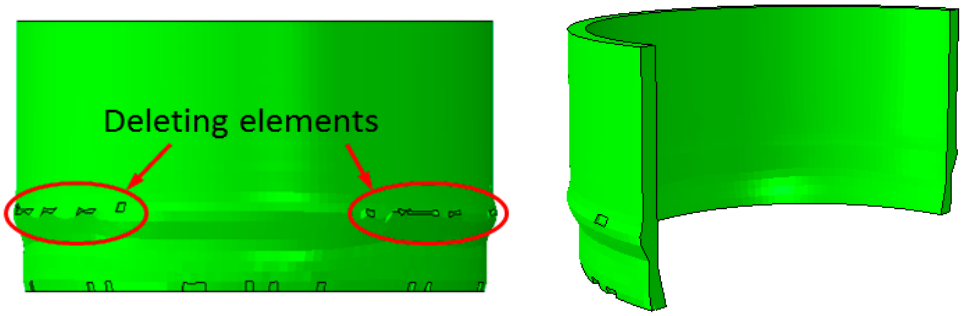

Figure 7. Crack defects in simulation in the (**a**) outer surface and (**b**) inner surface of tube at wall thickness reduction ratio of 50%.

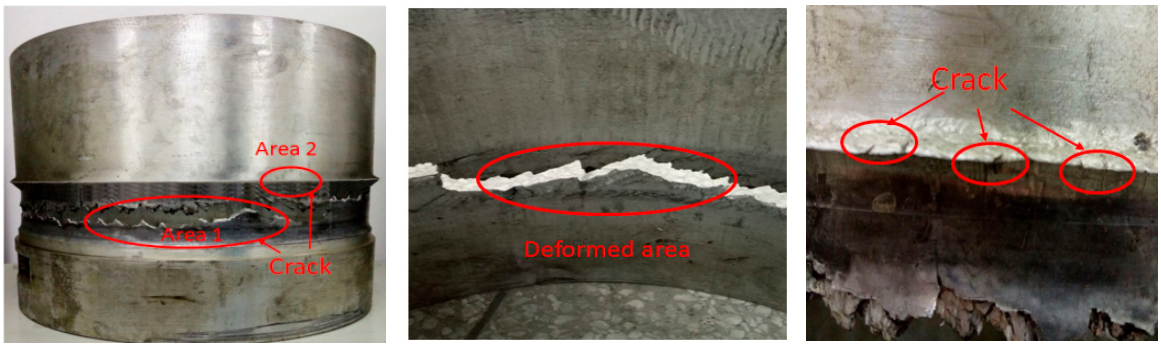

Figure 8. Crack defects of tube in experiment in the (**a**) outer surface; (**b**) inner surface and (**c**) magnified image of Area 2 in the outer surface of tube at wall thickness reduction ratio of 50%.

To analyze the discrepancy of the crack position between simulation and experiment results, Figure 9 shows the VVF distributions of two points, without crack (point A) and with crack (point B), respectively, in outer surface of spun tube at wall thickness reduction ratio of 50%. It can be seen that variations of VVF of the two points are similar to each other. Before spinning, there is no significant change of VVF. Then VVF increases sharply when the point is in the material uplift area. The maximum value of VVF of the point with crack can reach to 0.08. During spinning, VVF of the points decrease rapidly and values of it are close to zero at the end of spinning process. After spinning, values of VVF

are stable and keep to zero. The similar variation of damage evolution is also found in the researches of Ma *et al.* [7] by applied Ayada damage model for tube spinning. These indicate that, in GTN damage model for forward tube spinning, the void nucleation, growth and coalescence occurs in material uplift area, then the void is annihilated during spinning process under the compression of rollers.

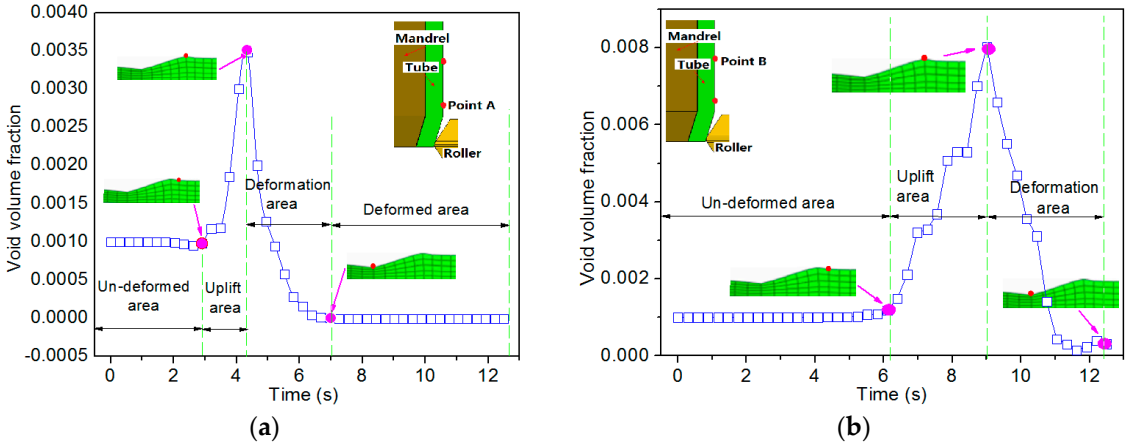

Figure 9. Distribution of void volume fraction (VVF) of the point (**a**) without crack and (**b**) with crack in forward tube spinning.

In GTN damage model, the characterization of damage evolution can be done by a combination of the stress triaxiality and Lode parameter [24]. Figure 10a,b show the variations of stress triaxiality of the two points during forward spinning process. It can be seen that, in the un-deformed area and uplift area, stress triaxiality is positive, which is good for damage accumulation. Then the stress triaxiality changes to negative in deformation area and finally changes to positive in deformed area. The variations of stress triaxiality of the two points in outer surface of spun tube are similar to researches of Ma *et al.* [7], where C-L ductile fracture criterion is employed to investigate the spinnability of tube. In general, GTN damage model or modified GTN damage model have a good performance in prediction fracture location under high stress triaxiality or shear loading [25,26]. However, the GTN damage model does not work well for uniaxial compression and plane strain compression since the void volume fraction does not increase due to the fact that void growth was suppressed in negative stress triaxiality [15]. Therefore, the GTN damage model could not precisely predict the variation of VVF in deformation area in forward tube spinning, and the variation of VVF in the subsequent deformed area is also influenced.

Meanwhile, in tube spinning, the deformed area is usually simplified as a plane strain state, namely compression deformation in radial direction and tensile deformation in axial direction. Figure 10c,d shows the variation of Lode parameter in spinning process. It can be seen that Lode parameter fluctuates widely during the whole process especially in deformation area and deformed area. In the un-deformed area, negative Lode parameter indicates there is mainly tensile deformation in this area. In uplift area, Lode parameter changes to positive gradually. Fluctuations of Lode parameter in these areas are influenced by the rapid variation of principal stresses under compatible deformation. In deformation area, the values of Lode parameter fluctuate from -0.6 to 0.4, and some values of Lode parameter are close to 0. The fluctuation of Lode parameter in deformation area is mainly resulted from the progressive deformation in spinning. When the point contacts to the roller, it undergoes shear-compression deformation; when the point is rotating to the area between the two rollers and still in the deformation area, it undergoes the addition shear-tension deformation. In addition, the degree of deformation gradually increases when the point contacts to roller again. Values of Lode parameter in deformation area indicate that the material in this area undergoes larger shear deformation than in other area of tube. In tube spinning, larger shear deformation is mainly generated

in circumferential direction by the transmission of torsional moment when the blank rotates with the mandrel. In deformed area, the reason for the fluctuation of Lode parameter is similar to it in un-deformed area and material uplift area. Therefore, the shear strain in circumferential direction is also important and shouldn't be neglected especially in deformation area. Under shear loads, failure is mainly driven by the shear localization of plastic strain of the inter-voids ligaments due to void rotation and distortion [27,28]. However, the shear strain is not taken account in the classical GTN damage model, which could results in some offset of the VVF variation in deformation area as well as the subsequent deformed area.

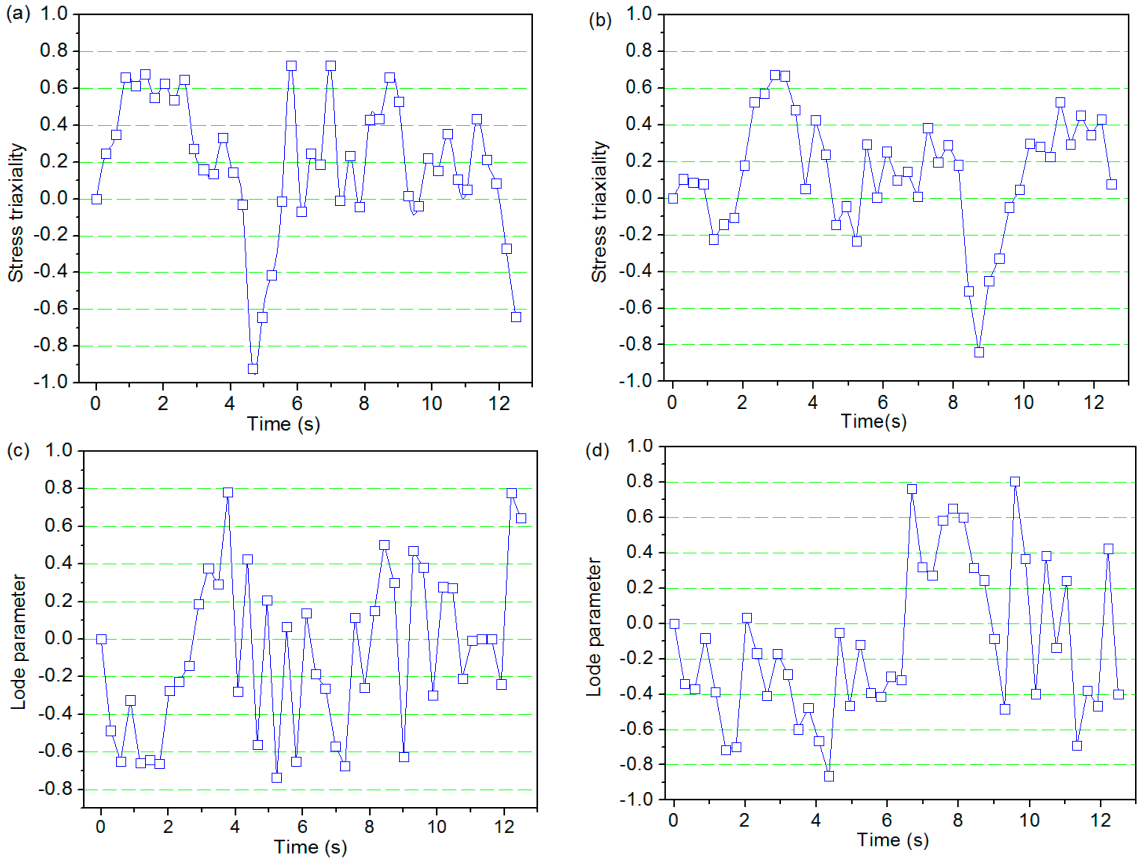

Figure 10. Distributions of stress triaxiality of the point (**a**) without crack; (**b**) with crack and lode parameter of the point (**c**) without crack and (**d**) with crack in forward tube spinning.

As explained above, the main reason for the failed prediction of the crack in deformed area is that the negative stress triaxiality and shear deformation in deformation area are not taken into consideration in the classical GTN damage model. Another reason is that, in simulation, when deformation occurs, the values of VVF are decreased and values of VVF after deformation are even smaller than the initial VVF. These mean that the macroscopic crack could be annihilated due to the dynamic change of VVF. While in experiment, once macroscopic crack appearing in tube, it is hard to eliminate but to expansion under complicated stress state. Initial crack seems to derive in the uplift area and then expansion to the deformed area leading to large cracks after severely deformation. Therefore, GTN damage model is available to predict the position of macroscopic crack appearing in the material uplift area in forward tube spinning.

5. Damage Evolution in Forward Tube Spinning

It is well known that the triaxiality stress, maximum principal stress and void volume fraction have a significance effect on damage evolution. Thus, based on the FE model coupled with GTN

damage model for forward tube spinning, distributions of stress triaxiality, maximum principal stress and void volume fraction are studied, as shown in Figure 11.

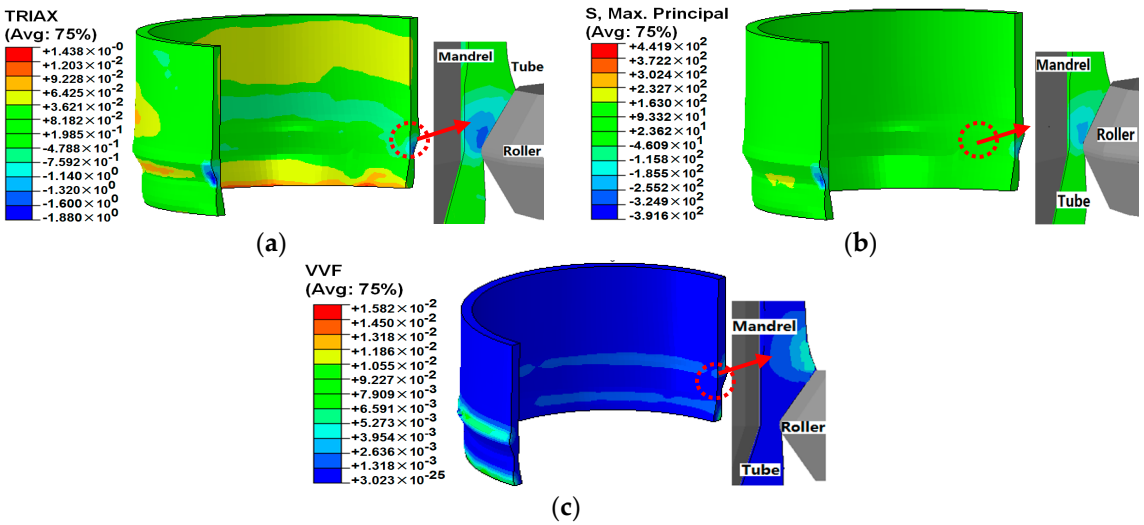

Figure 11. Distributions of (**a**) stress triaxiality; (**b**) maximum principal stress and (**c**) VVF in spun tube.

It can be seen that, in Figure 11a, the value of stress triaxiality near the upper surface of tube is close to zero due to the small compatible deformation produced in spinning; in the un-deformed area which is close to deformation area, the values of stress triaxiality change to positive. In material uplift area and deformed area, the value of stress triaxiality should be positive combined with the distributions of VVF of the points with crack and without crack (Figure 10a,b). In the deformation area contacting with roller, stress triaxiality is negative under the pressure of roller, which indicates that damage growth is restrained in this area. Neighboring areas in circumferential direction undergoes positive stress triaxiality due to the compressive deformation under the roller generating the additional tensile deformation in neighboring region. The positive stress triaxiality in the bottom surface of the tube is due to the coupling constraint applied in this surface. Characteristics of maximum principal stress in Figure 11b indicated that, in the roller contacting area (deformation area), the maximum principle stress can reach to approximately −250 MPa. The value of maximum principal stress in neighboring of roller contacting area in circumferential direction is positive due to the additional tensile deformation. Except for these areas, the maximum principle stress is close to zero because main deformation does not occur in other area of tube. Figure 11c shows the VVF distribution in the tube. It is found that: VVF in uplift area and bottom area of tube is close to 0.004 (VVF at fracture); while in other areas of the tube, the value of VVF is close to initial value of 0.001. Smaller values of VVF appear in un-deformed area because small deformation away from roller cannot lead to the increasing of VVF. In the un-deformed area near deformation area and uplift area, positive stress triaxiality results in the increasing of VVF. In the deformation area, material undergoes larger compression deformation and stress triaxiality are negative and VVF is decreased in this area. These result in the maximum VVF appearing in the uplift zone not in the deformation area. This means that GTN model could only capture the fracture occurred in material uplift area. Damage evolution in the deformation area and subsequent deformed area cannot be well predicted due to the decrease of VVF under negative deviation ratio. The distribution of lager VVF in uplift area in tube forward spinning is similar to the VVF distribution in spilt spinning in the research of Li *et al* [16]. Meanwhile, VVF in outer surface is higher than that in inner surface of spun tube. This indicates that cracks are easy to occur in the outer surface of the spun tube.

To observe the characteristics of damage evolution in the material uplift area clearly, the variation of stress triaxiality, maximum principal stress and VVF are obtained along four paths in radius direction

(Figure 12), as shown in Figure 13. It can be found that values of stress triaxiality decrease from inner surface to middle thickness section first, then increase and reach to maximum value of outer surface. This is due to the large amount of deformation in outer surface under the effect of roller and small amount of deformation under the friction between blank and mandrel in forward tube spinning. When the point is away from roller contacting area to uplift area, values of stress triaxiality gradually change from negative to positive. These indicate that in the uplift area, damage is easier to be accumulated, and cracks occur from the outer surface to inner surface on account of positive stress triaxiality. As we can see, the laws of maximum principal also show the tendency of decreasing slightly first and then increasing from the inner surface to outer surface (Figure 13b). The variations of void volume fraction along radial paths are obtained, as shown in Figure 13c. It can be found that, values of VVF in inner surface along different paths are close to each other. VVF is gradually increased when the path is away from the deformation area in outer surface. In addition, values of VVF in outer surface are greater than them in inner surface, which is resulted from accumulation of VVF under the positive stress triaxiality. This indicates that in the outer surface of material uplift area, the material is easy to crack when it is far away from rollers.

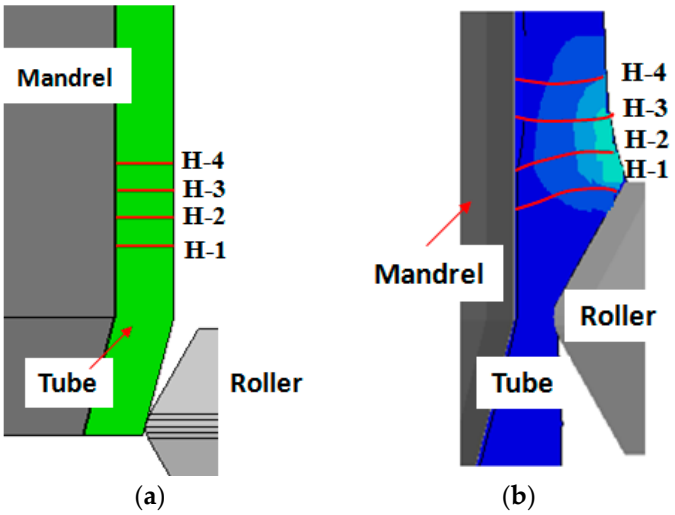

Figure 12. (**a**) Paths in tube blank and (**b**) paths in spun tube.

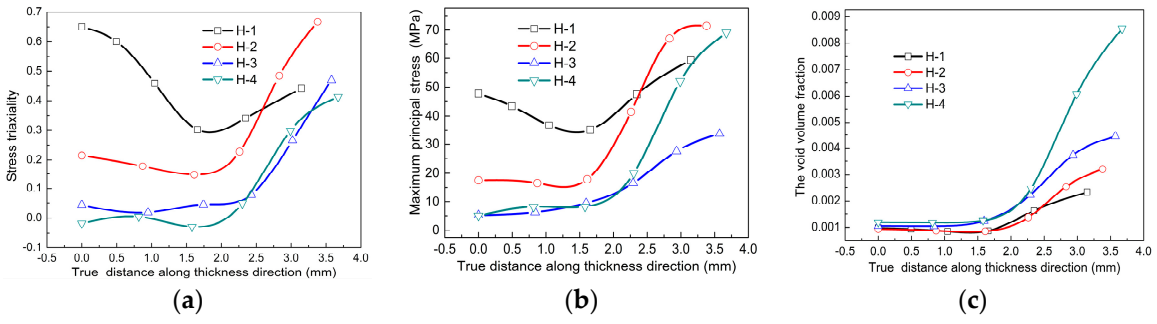

Figure 13. Distributions of (**a**) stress triaxiality; (**b**) maximum principal stress and (**c**) VVF in tube along the different radial paths.

According to the characteristics of stress triaxiality, maximum principal stress and void volume fraction, it can be concluded that accumulation of damage in tube spinning occurs mainly at the material uplift area. In addition, in the outer surface of material uplift area, the material is easy to crack when it is far away from rollers.

6. Conclusions

The applicability of GTN damage model in forward tube spinning of 3A21-O aluminum alloy is evaluated by experiment and the damage evolution is studied through analyzing the law of distribution of the stress triaxiality, the maximum principal stress, and the void volume fraction. The main results are as follows:

(1) Main parameters in GTN model, f_n, f_c and f_F of 3A21-O aluminum alloy, are determined 0.02, 0.012 and 0.04, respectively, by anti-inference method. A three-dimensional finite element numerical simulation model coupled the GTN damage model for forward tube spinning of 3A21 aluminum alloy is established. In addition, the GTN damage model is appropriate for predicting macroscopic crack in the material uplift area. The damage evolution in deformation area could not be predicted well with GTN damage model due to the negative stress triaxiality and the neglect of shear deformation.

(2) Accumulation of damage in forward tube spinning occurs mainly at the material uplift area through FE modeling. The VVF in the outer surface of the tube is higher than that in the inner surface in forward tube spinning. In addition, it is prone to cracking in the outer surface of tube in the material uplift area.

Acknowledgments: The authors would like to acknowledge the support from the National Science Fund for Excellent Young Scholars of China (Project 51222509), the National Natural Science Foundation of China (Project 51175429), the United Fund of Aerospace Advanced Manufacturing Technology (Project U1537203) and the Research Fund of the State Key Laboratory of Solidification Processing (Projects 97-QZ-2014 and 90-QP-2013).

Author Contributions: Xianxian Wang performed the experiments, simulations and wrote this paper under the guidance of Mei Zhan; Jing Guo and Bin Zhao assisted in performing experiments and analyzing simulation results.

Conflicts of Interest: The authors declare no conflict of interest.

Nomenclature

ϕ	Yield function
σ_{eq}	Von Mises equivalent stress
σ_y	Mean uniaxial equivalent stress of the matrix material
Σ_m	Macroscopic hydrostatic pressure
f	Void volume fraction
f^*	Modified void volume fraction
f_c	Critical void volume fraction
f_F	Void volume fraction at failure
F_n	Void volume fraction due to nucleation
F_g	Void volume fraction due to growth
S_n	Standard deviation of nucleation
q_1, q_2, q_3	Coefficients of the GTN damage model

References

1. Mohebbi, M.S.; Akbarzadeh, A. Experimental study and FEM analysis of redundant strains in tube spinning of tubes. *J. Mater. Process. Technol.* **2010**, *210*, 389–395. [CrossRef]
2. Xia, Q.X.; Xiao, G.F.; Long, H.; Cheng, X.Q.; Sheng, X.F. A review of process advancement of novel metal spinning. *Int. J. Mach. Tool. Manuf.* **2014**, *85*, 100–121. [CrossRef]
3. Music, O.; Allwood, J.M.; Kawai, K. A review of the mechanics of metal spinning. *J. Mater. Process. Technol.* **2010**, *210*, 3–23. [CrossRef]
4. Wong, C.C.; Dean, T.A.; Lin, J. A review of spinning, shear forming and flow forming processes. *Int. J. Mach. Tool Manuf.* **2003**, *431*, 1419–1435. [CrossRef]
5. Gur, M.; Tirosh, J. Plastic flow instability under compressive loading during shear spinning process. *Trans. ASME J. Eng. Ind.* **1982**, *104*, 17–22. [CrossRef]

6. Davis, J.R. *Metals Handbook*, 2nd ed.; ASM International: Russell, KS, USA, 2001.
7. Ma, H.; Xu, W.C.; Jin, B.C.; Shan, D.B.; Nutt, S.R. Damage evaluation in tube spinnability test with ductile fracture criteria. *Int. J. Mech. Sci.* **2015**, *100*, 99–111. [CrossRef]
8. Zhan, M.; Zhang, T.; Yang, H.; Li, L.J. Establishment of a thermal damage model for Ti-6Al-2Zr-1Mo-1V titanium alloy and its application in the tube rolling-spinning process. *Int. J. Adv. Manuf. Technol.* **2016**. [CrossRef]
9. Zhan, M.; Gu, C.J.; Jiang, Z.Q.; Hu, L.J.; Yang, H. Application of ductile fracture criteria in spin-forming and tube-bending processes. *Comput. Mater. Sci.* **2009**, *47*, 353–365. [CrossRef]
10. Gurson, A.L. Continuum theory of ductile rupture by void nucleation and growth. Part I. Yield criteria and flow rules for porous ductile media. *J. Eng. Mater. Technol.* **1977**, *99*, 2–15. [CrossRef]
11. Tvergaard, V.; Needleman, A. Analysis of the cup-cone fracture in a round tensile bar. *Acta Metall.* **1984**, *32*, 157–169. [CrossRef]
12. Chen, Z.Y.; Dong, X.H. The GTN damage model based on Hill' 48 anisotropic yield criterion and its application in sheet metal forming. *Comput. Mater. Sci.* **2009**, *44*, 1013–1021. [CrossRef]
13. Butcher, C.; Chen, Z.T.; Bardelcik, A.; Worswick, M. Damage-based finite-element modeling of tube hydroforming. *Int. J. Fract.* **2009**, *155*, 55–65. [CrossRef]
14. Sun, Q.; Zan, D.Q.; Chen, J.J.; Pan, H.L. Analysis of edge crack behavior of steel sheet in multi-pass cold rolling based on a shear modified GTN damage model. *Theor. Appl. Fract. Mech.* **2015**, *80*, 259–266. [CrossRef]
15. Nahshon, K.; Hutchinson, J.W. Modification of the Gurson model for shear failure. *Eur. J. Mech. A Solid* **2008**, *27*, 1–17. [CrossRef]
16. Li, H.; Fu, M.W.; Lu, J.; Yang, H. Ductile fracture: Experiments and computations. *Int. J. Plast.* **2011**, *27*, 147–180. [CrossRef]
17. Zhang, J.H.; Zhan, M.; Yang, H.; Jiang, Z.Q.; Han, D. 3D-FE modeling for power spinning of large ellipsoidal heads with variable thicknesses. *Compt. Mater. Sci.* **2012**, *53*, 303–313. [CrossRef]
18. Chu, C.C.; Needleman, A. Void nucleation effects in biaxially stretched sheets. *J. Eng. Mater. Technol.* **1980**, *102*, 249–256. [CrossRef]
19. Vadillo, G.; Fernández-Sáez, J. An analysis of Gurson model with parameters dependent on triaxiality based on unitary cells. *Eur. J. Mech. A Solid* **2009**, *28*, 417–427. [CrossRef]
20. Aravas, N. On the numerical integration of a class of pressure-dependent plasticity models. *Int. J. Numer. Methods Eng.* **1987**, *24*, 1395–1416. [CrossRef]
21. He, M.; Li, F.G.; Wang, Z.G. Forming limit stress diagram prediction of Aluminum alloy 5052 based on GTN model parameters determined by *in situ* tensile test. *Chin. J. Aeronaut.* **2011**, *24*, 378–386. [CrossRef]
22. Yan, Y.; Sun, Q.; Chen, J.; Pan, H. The initiation and propagation of edge cracks of silicon steel during tandem cold rolling process based on the Gurson-Tvergaard-Needleman damage model. *J. Mater. Process. Technol.* **2013**, *213*, 598–605. [CrossRef]
23. *ABQSUS Analysis User's Manual*; Version 6.8; ABAQUS. Inc.: Paris, France, 2008.
24. Lou, Y.S.; Huh, H. Prediction of ductile fracture for advanced high strength steel with a new criterion: Experiments and simulation. *J. Mater. Process. Technol.* **2013**, *213*, 1284–1302. [CrossRef]
25. Malcher, L.; Andrade Pires, F.M.; de Sá, J.M.A.C. An extended GTN model for ductile fracture under high and low stress triaxiality. *Int. J. Plast.* **2014**, *54*, 193–228. [CrossRef]
26. Xue, L. Constitutive modeling of void shearing effect in ductile fracture of porous materials. *Eng. Fract. Mech.* **2008**, *75*, 3343–3366. [CrossRef]
27. Chaboche, J.L.; Boudifa, M.; Saanouni, K. A CDM approach of ductile damage with plastic compressibility. *Int. J. Fract.* **2006**, *137*, 51–75. [CrossRef]
28. Kim, J.; Gao, X.S.; Srivatsan, T. Modeling of void growth in ductile solids: Effects of stress triaxiality and initial porosity. *Eng. Fract. Mech.* **2004**, *71*, 379–400. [CrossRef]